AIP Journal of Applied Physics

Coherent phonon modes of crystalline and amorphous Ge2Sb2Te5 thin films: A fingerprint of structure and bonding

A. Shalini, Y. Liu, F. Katmis, W. Braun, G. P. Srivastava, and R. J. Hicken

Citation: Journal of Applied Physics **117**, 025306 (2015); doi: 10.1063/1.4905617

View online: http://dx.doi.org/10.1063/1.4905617

View Table of Contents: http://scitation.aip.org/content/aip/journal/jap/117/2?ver=pdfcov

Published by the AIP Publishing

Coherent phonon modes of crystalline and amorphous $Ge_2Sb_2Te_5$ thin films: A fingerprint of structure and bonding

A. Shalini,[1] Y. Liu,[1] F. Katmis,[2] W. Braun,[2] G. P. Srivastava,[1] and R. J. Hicken[1]
[1]*Department of Physics and Astronomy, University of Exeter, Exeter EX4 4QL, United Kingdom*
[2]*Paul Drude Institute for Solid State Electronics, Hausvogteiplatz 5-7, 10117 Berlin, Germany*

(Received 3 September 2014; accepted 26 December 2014; published online 13 January 2015)

Femtosecond optical pump-probe measurements have been made upon epitaxial, polycrystalline, and amorphous thin films of $Ge_2Sb_2Te_5$ (GST). A dominant coherent optical phonon mode of 3.4 THz frequency is observed in time-resolved anisotropic reflectance (AR) measurements of epitaxial films, and is inferred to have 3-dimensional T_2-like character based upon the dependence of its amplitude and phase on pump and probe polarization. In contrast, the polycrystalline and amorphous phases exhibit a comparatively weak mode of about 4.5 THz frequency in both reflectivity (R) and AR measurements. Raman microscope measurements confirm the presence of the modes observed in pump-probe measurements, and reveal additional modes. While the Raman spectra are qualitatively similar for all three phases of GST, the mode frequencies are found to be different within experimental error, ranging from 3.2 to 3.6 THz and 4.3 to 4.7 THz, indicating that the detailed crystallographic structure has a significant effect upon the phonon frequency. While the lower frequency (3.6 THz) mode of amorphous GST is most likely associated with $GeTe_4$ tetrahedra, modes in epitaxial (3.4 THz) and polycrystalline (3.2 THz) GST could be associated with either $GeTe_6$ octahedra or Sb-Te bonds within defective octahedra. The more polarizable Sb-Te bonds are the most likely origin of the higher frequency (4.3–4.7 THz) mode, although the influence of Te-Te bonds cannot be excluded. The effect of high pump fluence, which leads to irreversible structural changes, has been explored. New modes with frequency of 3.5/3.6 THz in polycrystalline/amorphous GST may be associated with Sb_2Te_3 or $GeTe_4$ tetrahedra, while a 4.2 THz mode observed in epitaxial GST may be related to segregation of Sb. © *2015 AIP Publishing LLC*.
[http://dx.doi.org/10.1063/1.4905617]

I. INTRODUCTION

$Ge_2Sb_2Te_5$ (GST) is widely used for optical storage media and in phase change random access memory (PCRAM) that has the potential to replace conventional semiconductor memories. Its use in optical storage is based on the large difference in optical properties between the crystalline and amorphous states. These alloys are characterized by fast switching between the amorphous and crystalline state and their ability to endure more than 10^5 write-erase cycles.[1–4] Crystalline GST has two possible structures, hexagonal and a distorted rock-salt structure. Amorphization of cubic GST involves an unusual change of short range order that has been described in terms of an umbrella flip of Ge atoms between sites of octahedral and tetrahedral coordination and erasure of wrong bonds (Ge-Ge and Ge-Sb).[5,6] The coherent response of GST to optical excitation can be measured via changes in reflectivity (R). Although several studies have been performed of coherent optical phonons (COPs) in amorphous and polycrystalline GST films in the last two decades,[7–11] a comparison with measurements made on the epitaxial phase has not yet been reported. Epitaxial thin films provide new opportunities to understand the structure of crystalline GST and study the detailed structural changes that occur during the phase transition. Recently, it was demonstrated that epitaxial cubic GST films could be successfully grown on GaSb (001) and (111) substrates by molecular beam epitaxy.[12,13]

In a time-resolved ultrafast optical study of epitaxial cubic-$Ge_2Sb_2Te_5$/GaSb (001), anisotropic reflectance (AR) measurements revealed a dominant phonon mode of 3.4 THz frequency.[14] The dependence of the amplitude on pump and probe polarization was well described by a theory that includes phonon excitation by both transient stimulated Raman scattering (TSRS) and a space charge (SC) field. The theory, which includes the crystal symmetry through the Raman tensor, revealed that the 3.4 THz mode has a three-dimensional T_2-like character, confirming the view that the underlying crystallographic structure is cubic.

In this paper, the transient R and AR response[15] of the polycrystalline and amorphous phases of GST thin films to an intense femtosecond laser pulse are investigated by means of a time-resolved optical pump-probe technique. The results are compared to the R and AR responses of an epitaxial sample described previously[14] and with Raman spectra obtained from the three samples. THz optical phonons of different frequencies have been observed in the three different phases, helping to advance understanding of the crystal structure and phase transition in GST.

II. SAMPLE DETAILS AND EXPERIMENTAL METHOD

The samples used in this study were as-deposited polycrystalline (37 nm) and amorphous (57 nm) GST thin films grown on SiO_2(15 nm)/Si(001) substrates at 200 °C and at

20 °C, respectively. X-ray diffraction measurements performed on the polycrystalline sample were consistent with cubic rather than hexagonal structure, while the Raman spectrum acquired from the sample was similar to a spectrum published previously for cubic GST.[16] R and AR signals from these samples were compared with those from an epitaxial $Ge_2Sb_2Te_5$ (15 nm)/GaSb (50–100 nm)/GaSb (001) structure. The epitaxial GST film was grown at 200 °C on homoepitaxial GaSb (001) and found to have a predominantly cubic on cubic growth behaviour with the GST [100] axis parallel to the GaSb [100] axis.[12] The prefixes e, p, and a will be used to refer to the epitaxial, polycrystalline, and amorphous phases, respectively.

Time-resolved R and AR (optical rotation) measurements were performed upon GST thin films in an all-optical pump-probe configuration using femtosecond pulses from a Ti:Sapphire regenerative amplifier.[14] The film was pumped with the linearly polarized 800 nm wavelength output of the regenerative amplifier at near normal incidence with pulse fluence of 0.85 mJ/cm^2, and probed by an s-polarized 800 nm probe beam incident at 45° with a smaller pulse fluence of 0.2 mJ/cm^2. The probe was focused so as to overlap with the pump spot on the sample surface. A beam profiler[17] was inserted at the sample position to obtain optimum overlap of pump and probe beams. The intensity profiles of the spots along their principal axis were observed to be Gaussian. The sizes of the pump and probe spots defined by the $1/e^2$ intensity level were $100\,\mu m \times 120\,\mu m$ and $30\,\mu m \times 40\,\mu m$, respectively. The pulse duration was adjusted inside the compressor stage of the amplifier so as to have minimum values for both pump and probe beams at the sample position, and was measured to be 50 ± 2 fs using an autocorrelator. The intensity of the pump beam was modulated by a mechanical chopper, while the induced changes in intensity and polarization of the reflected probe beam were detected by an optical bridge detector combined with two lock-in amplifiers. Within the optical bridge a polarizing beam splitter separates the probe beam into two components with orthogonal polarization, and their intensities are measured simultaneously by two photodiodes. The sum of these two signals yields the transient R, while the difference yields the transient AR (rotation of polarization). Measuring both transient R and AR simultaneously provides additional information that assists identification of observed phonon modes, and understanding of the mechanisms by which they are excited and detected.

In the experimental setup used in this study, the probe beam was always s-polarized, while the pump polarization and the sample could be rotated independently, so that the dependence of the transient R and AR upon the polarization of the pump and probe beams could be studied. Measurements of transient AR must be performed with great care to avoid the appearance of artefacts within the acquired data. The probe beam must be set precisely to the s-polarized state, and the sample normal must be exactly parallel to the plane of the optical table so that the reflected probe beam does not precess as the sample is rotated around its normal. The bridge detector must be carefully balanced so as to avoid breakthrough of the transient R signal into the AR signal, and the pulses must be unchirped when they arrive at the sample or else strong variations of the AR signal may be induced close to zero time delay.

III. EXPERIMENTAL RESULTS

A. Pump-probe measurements at low pump fluence

The transient R and AR responses of all three samples in experiments performed with low pump fluence are shown in Figure 1 for comparison. Figures 1(a)/1(b) show the AR/R response of the e-GST film for the pump electric field polarized parallel to the GaSb [110] axis and the probe polarization parallel to the [100] axis. The amplitude of the oscillations associated with the COPs is found to be larger in this case than when the pump polarization is parallel to the cube edge. Also, it is important to notice that the pump and probe polarizations lie 45° apart. The AR/R responses for the p-GST film and the a-GST film are presented in Figures 1(c)/1(d) and 1(e)/1(f), respectively. The AR signal contains a variety of features on a wide range of different time scales, and so has been plotted on both fs (main panel) and longer time scales (two insets). The AR signal clearly reveals three important features: (i) a large peak on fs time scales with a Gaussian profile that sits approximately within the temporal overlap of the pump and probe pulses; (ii) oscillatory components on time scales of order 1 ps superimposed on a background; and (iii) a longer-lived tail (ns scale).

All three samples exhibit a sharp initial peak with maximum amplitude when the pump and probe polarizations are +/−45° apart. The peak vanishes when the pump and probe polarizations are either parallel or orthogonal. Throughout the measurements on the a/p-GST samples, the probe polarization was kept fixed along Si[110] and the polarization of the pump, at normal incidence, was rotated to change the angle between the pump and probe electric fields. This initial peak is associated with optical modification of the electron momentum distribution. The linearly polarized pump beam transfers linear momentum to electrons in the surface of the sample, and so generates a transient linear birefringence known as the specular optical Kerr effect (SOKE). The width of the SOKE peak is close to 100 fs in all three samples, and appears similar to an autocorrelation of the pulse in most materials. In fact, the precise form of the pump induced transient polarization signal contains information about the rate of relaxation of the linear momentum of the excited electrons.[18]

Oscillations superimposed upon a background are observed in both the AR and R signals on time scales of order 1 ps. The AR response of e-GST is significantly more complicated than that of p/a-GST, in part because of the more strongly featured response of the GaSb (001) substrate. The e-GST response was fitted to a function consisting of a Gaussian function to describe the initial peak, a series of Gaussian error functions to describe the multi-exponential background, and cosine functions to describe the oscillatory response, as has been described previously.[14] The fitting yielded two strong oscillatory signals and various relaxation times associated with the complicated background that were carefully assigned to carrier-carrier and carrier-phonon interaction processes, and to the decay of a space charge field

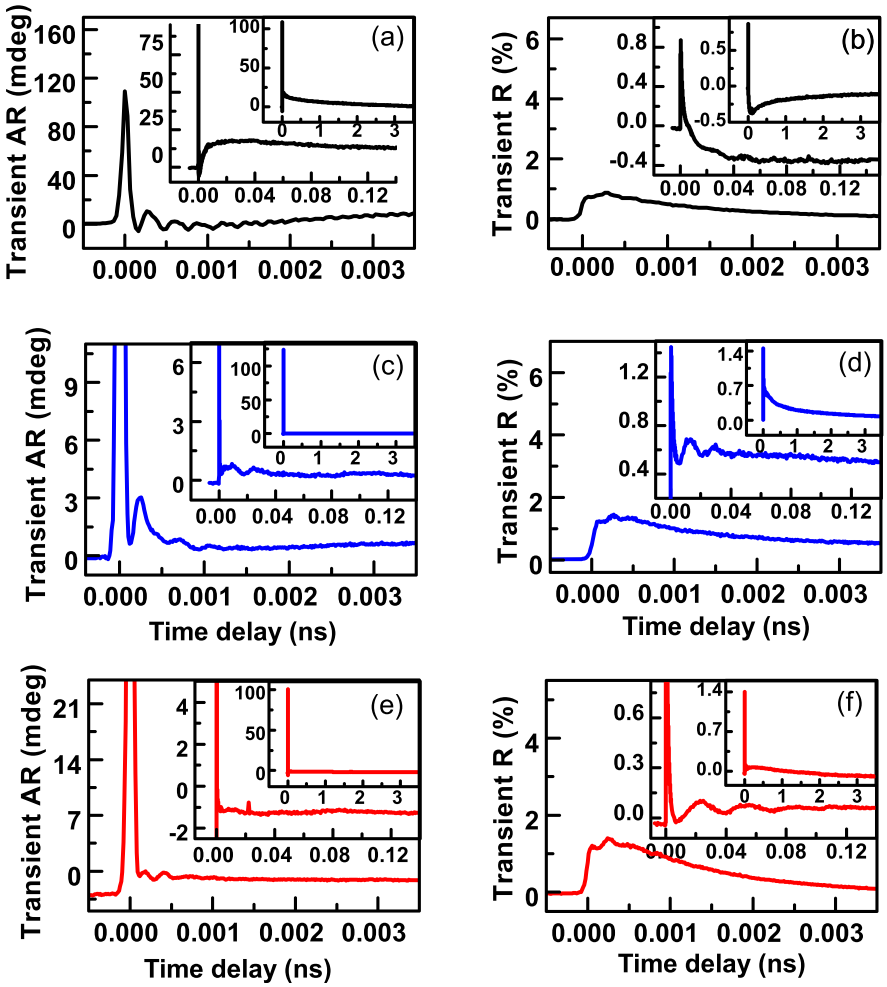

FIG. 1. Typical pump probe signals: (a)/(b) show the AR/R response of the e-GST film for pump polarization along the GaSb [110] axis and probe polarization along the [100] axis; (c)/(d) present the AR/R response of the p-GST film; while (e)/(f) show the AR/R response of the a-GST films. The pump and probe polarizations lie 45° apart in (c)–(f).

within the piezoelectric GaSb.[14] One of the oscillatory signals with frequency of 6.77 THz is associated with the GaSb substrate. The other oscillatory signal of 3.4 THz frequency arises from the e-GST film. Its amplitude exhibited a four-fold dependence on the orientation of the probe polarization but was found to have weak or no dependence upon the orientation of the pump polarization.

The AR response of p/a-GST contains oscillations of smaller amplitude and larger damping compared to e-GST, superimposed on a background that is significantly simpler due to the absence of a piezoelectric response in the substrate. The frequency of oscillation was determined by taking the data immediately after the SOKE peak, subtracting a fit to the slowly varying background, and then calculating the Fast Fourier Transform (FFT) of the residual. In both cases, a clear peak was observed in the power spectrum, the centre frequency and linewidth of which was determined by fitting to a Lorentzian lineshape. In each case, the centre frequency was found to lie close to 4.5 THz.

A similar procedure was used to fit the oscillations observed in the R signals, but using all of the data from negative to positive delay times. The oscillatory signals are weaker and more heavily damped compared to those observed in the AR signal and so give rise to larger fitted linewidths. Taking into account the error in the fitted centre frequency and the large linewidths, it appears that the oscillation frequency lies close to 4.5 THz in all three samples. It is interesting to note that the oscillations in the R signal have a similar appearance for all three samples and that no obvious dependence upon pump and probe polarization was observed. However, the 3.4 THz mode did not appear in the transient R response of the e-GST sample.

The frequencies of oscillation in the epitaxial sample were also extracted by calculating the FFT of the residual after subtraction of the fitted background. The centre frequencies and linewidths were determined by fitting two Lorentzian functions to the FFT power spectrum. The linewidth of the 3.4 THz mode determined by this method could then be directly compared with the linewidths determined for the polycrystalline and amorphous films.

B. Pump-probe measurements at increased pump fluence

The effect of increased pump fluence upon the transient R and AR signals obtained from e-GST was reported previously[14] and has been investigated in the present study for p/a-GST films. The transient R and AR signals were recorded at high fluence, over a period of about 40 min, before being remeasured at the same location on the sample using a reduced pump fluence. This measurement procedure was

used to detect irreversible structural transitions that may occur during exposure to high pump fluence.

Figures 2(a)/2(b) show the effect of pump fluence on the transient AR/R signals obtained from the p-GST sample, while Figures 3(a)/3(b) show the effect of pump fluence for the amorphous sample. At low pump fluence (<2.12 mJ/cm^2), the polycrystalline and amorphous GST films exhibit quite similar behaviour to that observed for e-GST. First, the peak heights of the transient R and AR signals were observed to increase linearly with pump fluence for the full range of pump fluence studied. Second, only a few periods of oscillation with frequency of 4.5 THz were observed in the R signal at low pump fluence prior to structural changes being induced by a high pump fluence. Figs. 2(c)/2(d) and 3(c)/3(d) show the oscillatory components in the transient AR/R signals obtained from the p-GST and a-GST samples, respectively, with low pump fluence (0.42 mJ/cm^2) after exposure to high pump fluence. Figs. 2(e)/2(f) and 3(e)/3(f) show the power spectra of the transient AR/R signals obtained from the p-GST and a-GST samples, respectively. For low pump fluence rescans after exposure to fluences in excess of 2.12 mJ/cm^2, the COP with frequency of 4.5 THz in p/a-GST became weak and eventually disappeared. Instead, a COP with frequency of 3.52 ± 0.01 (3.54 ± 0.01) THz in p-GST and 3.61 ± 0.01 (3.64 ± 0.02) THz in a-GST was observed in R (AR) signals, the frequencies being obtained by fitting Lorentzian curves to the power spectra in each case.

C. Raman measurements

Micro-Raman measurements were performed on all three samples to check for the presence of the modes observed in the pump-probe measurements, and to gather more information about other modes observable within the samples. A laser beam of 785 nm wavelength at normal incidence to the sample was focused to a circular spot of 20 μm diameter, with the same microscope objective being used to collect the back-scattered light. Elastically scattered light in the reflected beam was removed by a filter, allowing only inelastically scattered light to reach the diffraction grating and detector. A polarizer and an analyzer were placed in the incident and scattered light paths, respectively, but the Raman spectra were found to be insensitive to their relative orientation. The system was also equipped with a conventional microscope path, which can image the sample area being investigated with the Raman probe. A measurement was made on a standard Si sample before making the measurements on the samples of interest, with a peak of 15.6 THz frequency being used to calibrate the system. The Raman spectra obtained from all three samples are presented in Figure 4 for comparison. The spectra exhibit a strong similarity with peaks of greater intensity appearing in a broad band between 2 and 6 THz. While the p/a-GST spectra show only a slowly varying background at large wavenumbers, the e-GST spectrum contains an additional peak at 7.08 THz, which

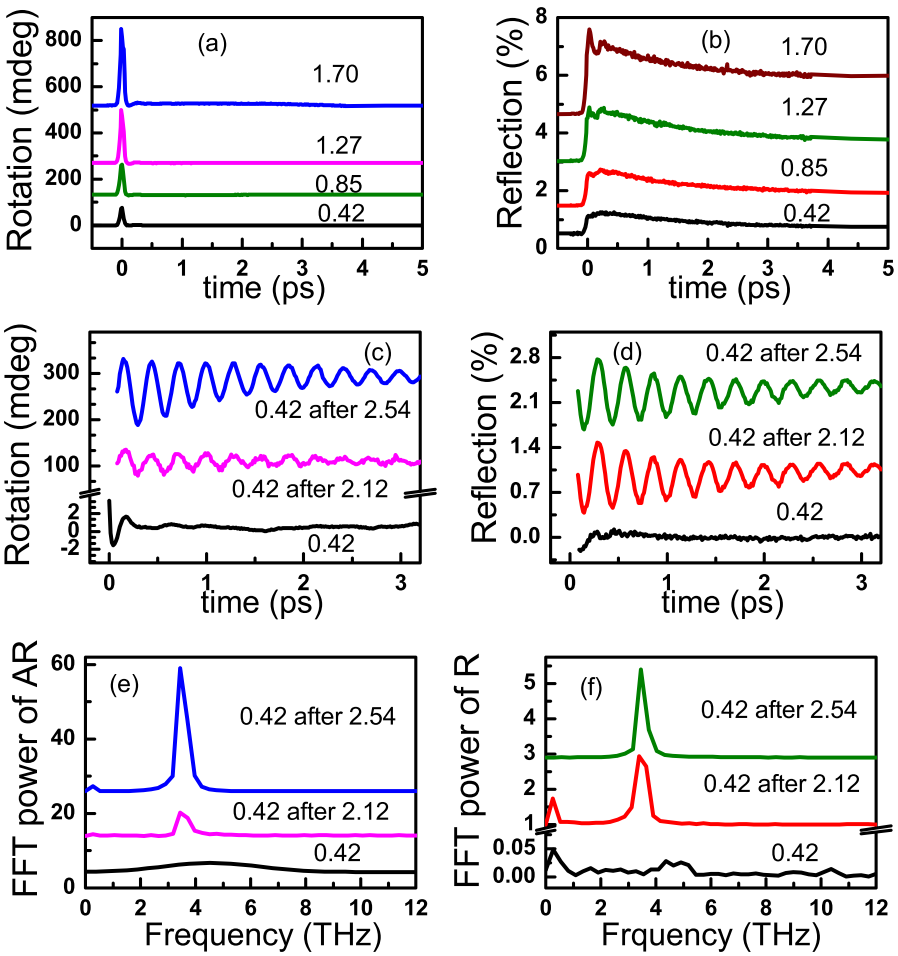

FIG. 2. Effect of pump fluence on transient R and AR signals obtained from p-GST. (a) and (b) Dependence of AR and R signals, respectively, upon pump fluence. (c) and (d) oscillatory components of AR and R signals, respectively, obtained with pump fluence of 0.42 mJ/cm^2 after exposure to the increased pump fluence used to label each curve. (e) and (f) power spectra of the AR and R signals from (c) and (d), respectively.

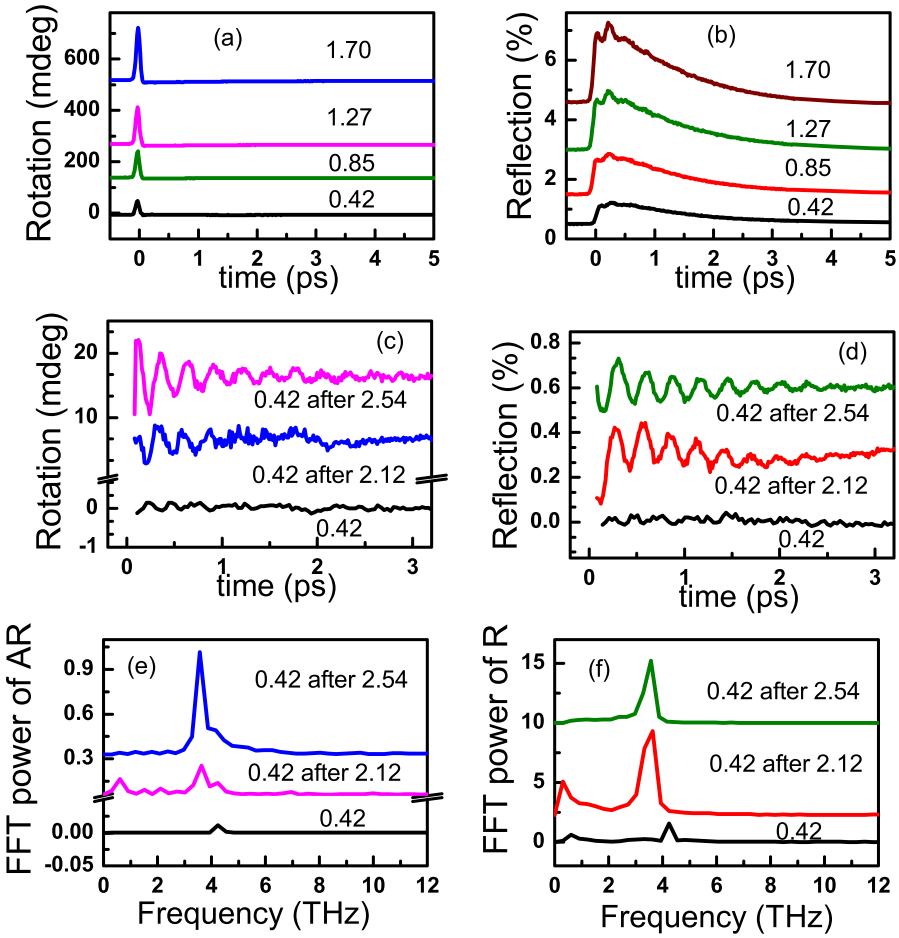

FIG. 3. Effect of pump fluence on transient R and AR signals obtained from a-GST. (a) and (b) Dependence of AR and R signals, respectively, upon pump fluence. (c) and (d) oscillatory components of AR and R signals, respectively, obtained with pump fluence of 0.42 mJ/cm^2 after exposure to the increased pump fluence used to label each curve. (e) and (f) power spectra of the AR and R signals from (c) and (d), respectively.

was also observed for a reference GaSb sample. Pump-probe measurements revealed a mode with a slightly lower frequency of 6.77 THz in the GaSb reference sample.[14] The modes observed in GaSb by Raman and pump-probe measurements are attributed to the zone centre LO and TO phonons, respectively.[19] The broad band between 2 and 6 THz was analyzed by first subtracting a sloping background, the physical origin of which is not known, and then fitting to two Lorentzian lineshapes, as shown in Figure 5.

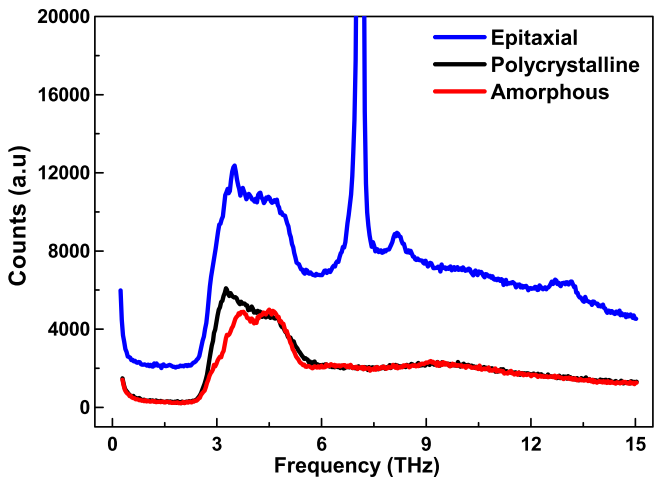

FIG. 4. Raman spectra obtained from e/p/a-GST samples.

IV. DISCUSSION

The mode frequencies and linewidths obtained from both pump-probe and Raman measurements are displayed in Table I for comparison. The Raman spectra of all three samples display a broad band between 80 and 180 cm^{-1} wavenumber (2.4 and 5.4 THz frequency) with two strong peaks, one close to 110 cm^{-1} (3.3 THz) and the other around 150 cm^{-1} (4.5 THz). The lower frequency modes observed in the Raman spectra of the p/a-GST samples were not observed in the pump-probe measurements on the same samples. However, both modes observed in the Raman spectrum of the e-GST sample were seen in the pump-probe experiments, with the 3.4 THz mode appearing in the AR signal and the weak 4.5 THz mode appearing in the R signal. For each sample, the frequencies obtained from Raman and pump-probe measurements agree within experimental error.

Although the phonon modes of a crystalline solid depend upon its long-range crystallographic structure, they are frequently interpreted in terms of the modes of simpler structural sub-units that retain their local coordination. The Raman spectra obtained from the three samples in the present study have a strong qualitative similarity, with the frequencies observed for the different samples being similar yet distinct. This suggests the presence of similar bonds within the different structural environments found within each sample. The Raman spectra for the e-/p-/a-GST samples each display frequencies close to 3.3 and 4.5 THz and are largely similar to Raman spectra reported in the literature.[12,16,20,21]

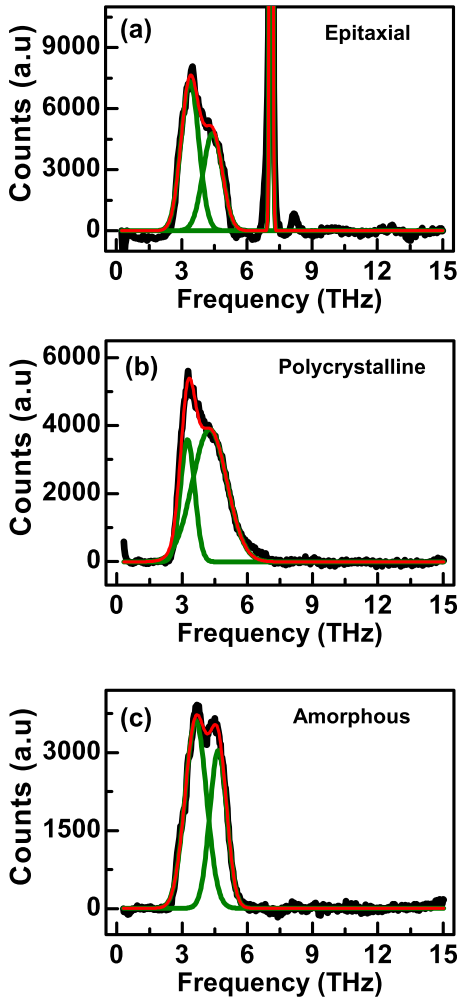

FIG. 5. Multipeak fitting of the Raman spectra, after subtraction of a sloping background, for (a) the e-GST sample, (b) p-GST, and (c) a-GST samples, respectively. The red curves show the superposition of the green Lorentzian curves in each spectrum.

The characteristic modes of crystalline and amorphous GST detected by time resolved pump-probe measurements have also been reported previously.[7–9] Först *et al.*[7] compared the coherent phonon spectra of amorphous and polycrystalline GST with those of amorphous GeTe and polycrystalline Sb_2Te_3, respectively. The coherent phonon spectra of a-GST and a-GeTe were found to be similar, both exhibiting two modes with similar frequencies (at about 3.7 and 4.8 THz) and relative amplitudes. This was attributed to the similar short-range order in a-GST and a-GeTe, leading to excitation of similar local phonon modes. Analysis of Raman data for a-GST and a-GeTe again confirmed the similarity of their amorphous phases.[16] Först *et al*. found the coherent phonon spectrum of p-GST to be similar to that of p-Sb_2Te_3[7] with principal mode frequencies at 2.0, 3.5, and 5.1 THz, but these frequencies differ significantly from those observed by both pump-probe and Raman measurements in the present study. Strictly speaking, the results of Först *et al*. should be compared only with the transient R measurements of the present study. Even then, the frequencies of the dominant modes are seen to disagree. It is possible that this is a consequence of the films in the two studies having different texture.

From a detailed first-principles theoretical study that included a bond polarizability model, Sosso *et al.*[20] concluded that the Raman peaks in both crystalline (c-GST) and a-GST can be assigned to vibrations of defective octahedra. They found that only Ge is tetrahedrally coordinated within the amorphous phase. However, since the Sb-Te bonds are more polarisable than the Ge-Te bonds, they suggested that modes associated with $GeTe_4$ tetrahedra are hidden in the Raman spectrum of a-GST because vibrations of defective octahedra have larger Raman cross-section. Furthermore, they found the Raman spectrum of a-Sb_2Te_3 to be very similar to that of a-GST, supporting the view that the Sb-Te bonds of defective octahedra dominate the spectrum of a-GST. However, their spectrum for a-GST did not contain the large peak at 3.6 THz that was observed in the present study. We suggest that this lower frequency (3.6 THz) mode of a-GST is in fact associated with the A_1 mode of $GeTe_4$ tetrahedra[7,8] In fact, it has been predicted[22] that tetrahedra are more prevalent in as-deposited samples, such as the a-GST sample studied here, while they were observed[23] to be less common in melt quenched and ion irradiated samples. A greater incidence of tetrahedra may also lead to more Te-Te bonds, and hence a mode at 3.6 THz as observed in the Raman spectra of Te precipitated from Te-rich GeTe alloys.[24] The lower frequency (3.2 THz) mode of p-GST could be associated with the A_1 mode of $GeTe_6$ octahedra, reflecting the local structural change from tetrahedral coordination in a-GST to octahedral coordination in c-GST.[9] The lower frequency (3.4 THz) mode of e-GST was previously deduced to be T_2-like, possessing a three dimensional character that might also be expected for the local vibrational modes of $GeTe_6$ octahedra. Thus, the downward frequency shift from 3.6 THz for a-GST to 3.4 THz for e-GST would again reflect a change from the

TABLE I. Comparison of pump-probe and Raman frequencies (in THz) obtained from the e/p/a-GST samples. Pump-probe frequencies were obtained by fitting the FFT power spectra of the time domain data, while multi-peak fitting was applied to the Raman spectra of all three samples.

Experiment		Epitaxial Frequency, linewidth	Polycrystalline Frequency, linewidth	Amorphous Frequency, linewidth
Pump-probe	AR	3.4 ± 0.1, 0.60 ± 0.04	4.6 ± 0.3, 1.11 ± 0.38	4.5 ± 0.3, 0.31 ± 0.05
	R	4.5 ± 0.3, 2.1 ± 0.25	4.7 ± 0.4, 6.9 ± 0.66	4.5 ± 0.3, 1.20 ± 0.11
Raman		3.37 ± 0.02, 0.78 ± 0.02	3.24 ± 0.04, 0.63 ± 0.01	3.60 ± 0.02, 0.96 ± 0.01
		4.42 ± 0.02, 1.08 ± 0.04	4.31 ± 0.03, 1.56 ± 0.02	4.62 ± 0.02, 0.78 ± 0.01
Pump-probe after high fluence	AR	4.21 ± 0.01, 0.76 ± 0.05	3.54 ± 0.01, 0.52 ± 0.02	3.64 ± 0.02, 0.82 ± 0.06
	R	4.23 ± 0.02, 0.77 ± 0.03	3.52 ± 0.01, 0.52 ± 0.02	3.61 ± 0.01, 0.75 ± 0.06

local tetrahedral ($GeTe_4$) to local octahedral ($GeTe_6$) configuration. On the other hand, the lower frequency mode of p-GST has also been discussed in terms of the degenerate E_g mode arising from the vibration of atoms orthogonal to the c-axis of a Sb_2Te_3 sub-unit,[7,8] and is associated with Sb-Te bonds in the study of Sosso *et al.*[20] Given the similarity of the Raman spectra for the three phases in the present study, and the similarity of frequencies associated with Ge-Te bonds in $GeTe_6$ and Sb-Te bonds in the Sb_2Te_3 sub-unit, we suggest that further detailed theoretical studies based on possible structural models are needed to resolve the exact origin of this mode.

The higher frequency mode of p-GST (4.6 THz) has previously been attributed to the symmetric A_{1g} mode of vibration of the Sb and Te layers along the c-axis of Sb_2Te_3. It is also known that the high-frequency optic mode in trigonal crystalline (ordered chain structure), polycrystalline, and amorphous (distorted chain structure) Te lies at $134\,cm^{-1}$ (4.02 THz), $143\,cm^{-1}$ (4.29 THz), and $150\,cm^{-1}$ (4.5 THz), respectively.[25] Given the similarity in the frequencies of the A_{1g} mode of Sb_2Te_3 and the chain mode in the Te structure, we again suggest that theoretical studies based on plausible atomic geometries should be undertaken to ascertain the precise origin of this mode in both a- and c-GST. Since essentially the same frequency (about 4.5 THz) is observed for all three phases, it seems natural to associate this mode with the same bond in each case. However, the calculations of Ref. 20 have shown that, within GST, different bonds give rise to modes of similar frequency. The fact that different structural phases give rise to similar excitation spectra may therefore be a defining feature of a good phase change material.

In pump-probe measurements made at high pump fluence, both polycrystalline and amorphous GST initially reach high temperatures, and so the new frequencies observed for p/a-GST in low fluence rescans are expected to have a similar origin. It is known that crystallization of a-GST by fs pulses[26] is very sensitive to the details of the sample stack. The presence of a capping layer or underlayer or a difference in sample thickness, can significantly modify heat flow within the sample. Therefore, the slight difference in the frequencies observed for low fluence rescans of p/a-GST is not necessarily surprising. As mentioned before, the sharp peak at 3.54/3.61 THz in p/a GST could be identified either as the degenerate E_g mode of crystalline Sb_2Te_3 (for which atoms in the outer Sb and Te layers vibrate perpendicular to the c-axis[7]) or with Te-Te bonds[25] or with the A_1 mode of $GeTe_4$ tetrahedra. Alternatively, it may indicate a transition to hexagonal order since a broad mode centred at 3.4 THz was predicted[27] for a certain hexagonal stacking sequence and found to be in reasonable agreement with experimental Raman spectra.[28] As yet another alternative, the observed mode could be associated with the E_g modes of crystalline Sb, which may form locally where high pump fluence has been applied.[10] In the first two cases, it is unclear why the mode was not observed with similar amplitude prior to exposure to high pump fluence, although it is possible that high pump fluence significantly increases the presence of distorted Te-Te chains and/or Sb-Te bonds within defective octahedra. Further work is required to make a definitive assignment for the origin of this mode.

While the mode observed in low fluence rescans of p/a-GST after the application of high fluence is shifted to lower frequency, e-GST shows a different behaviour.[14] The 3.4 THz mode in e-GST was observed to disappear, while a new mode with frequency of 4.2 THz was obtained from a low fluence rescan after exposure to fluence $\geq 2.12\,mJ/cm^2$. While the GaSb substrate may lead to a different transient temperature profile within the GST layer, it could also act as an additional source of Sb if the 4.2 THz mode is in fact associated with Sb segregation.

V. CONCLUSIONS

Comprehensive optical pump-probe measurements of three different structural phases of GST were performed under similar experimental conditions. The transient R and AR responses of the p/a-GST samples are much simpler than those of e-GST. e-GST exhibits a mode of 3.4 THz frequency that appears only in the transient AR response. The dependence of the amplitude of this mode upon the pump and probe polarization suggests a T_2-like character. The R signal contained oscillations with frequency close to 4.5 THz. A mode with similar frequency was also observed in the transient R and AR response of the p/a-GST samples. Raman spectra obtained from the three types of sample have a strong qualitative similarity, with frequencies ranging from 3.2 to 3.6 THz and 4.3 to 4.7 THz that are similar yet distinct. The Raman spectra confirm the modes observed in the pump-probe measurements, but also reveal other modes. We suggest that the lower frequency (3.6 THz) mode in a-GST is associated with $GeTe_4$ tetrahedra, while the lower frequency mode of p-GST (3.2 THz) and e-GST (3.4 THz) might be associated with $GeTe_6$ octahedra. However, for e/p-GST this mode could equally well originate from the more polarizable Sb-Te bonds. The higher frequency (4.3–4.7 THz) mode observed within the three samples is most likely also associated with Sb-Te bonds although a contribution from Te-Te bonds cannot be excluded. The continuing uncertainty about the origin of the observed modes argues for further theoretical work, in which phonon spectra of realistic structures are calculated. The fact that different structural phases appear to give rise to similar excitation spectra could be seen as a defining feature of a good phase change material. Exposure to higher pump fluence causes oscillations at 4.5 THz to be replaced with stronger oscillations at 3.5 and 3.6 THz for p-GST and a-GST, respectively. This suggests a new mode similar to the degenerate E_g mode of c-Sb_2Te_3 or perhaps the formation of $GeTe_4$ tetrahedra. The small difference in the frequencies observed for p-GST and a-GST after exposure to high fluence may result from differences in the sample stack that affect the time dependent temperature profile within each sample. For e-GST, the modes at 3.4 and 4.5 THz are replaced by a mode at 4.2 THz that could be associated with Sb segregation, possibly with Sb being released from the GaSb substrate. In summary, when taken together, the low fluence pump-probe and Raman measurements performed upon three phases of GST reveal modes that are similar but

distinct within experimental error, suggesting the presence of similar bonds subject to different structural environments.

ACKNOWLEDGMENTS

The authors gratefully acknowledge D. Lubert-Perquel and J. Di Trapani for assistance with sample characterisation and the financial support of the Engineering and Physical Sciences Research Council through Grant No. EP/F015046/1.

[1]N. Yamada, E. Ohno, K. Nishiuchi, N. Akahira, and M. Takao, J. Appl. Phys. **69**, 2849 (1991).
[2]M. Wuttig and N. Yamada, Nat. Mater. **6**, 824 (2007).
[3]D. Lencer, M. Salinga, B. Grabowski, T. Hickel, J. Neugebauer, and M. Wuttig, Nat. Mater. **7**(12), 972 (2008).
[4]J. Hegedüs and S. R. Elliott, Nat. Mater. **7**, 399 (2008).
[5]A. V. Kolobov, P. Fons, A. I. Frenkel, A. L. Ankudinov, J. Tominaga, and T. Uruga, Nat. Mater. **3**, 703 (2004).
[6]D. Lencer, M. Salinga, and M. Wuttig, Adv. Mater. **23**, 2030 (2011).
[7]M. Först, T. Dekorsy, C. Trappe, M. Laurenzis, H. Kurz, and B. Béchevet, Appl. Phys. Lett. **77**, 1964 (2000).
[8]M. Hase, Y. Miyamoto, and J. Tominaga, Phys. Rev. B **79**, 174112 (2009).
[9]K. Makino, J. Tominaga, and M. Hase, Opt. Express **19**, 1260 (2011).
[10]Y. Li, V. A. Stoica, L. Endicott, G. Wang, C. Uher, and R. Clarke, Appl. Phys. Lett. **97**, 171908 (2010).
[11]J. Hernandez-Rueda, A. Savoia, W. Gawelda, J. Solis, B. Mansart, D. Boschetto, and J. Siegel, Appl. Phys. Lett. **98**, 251906 (2011).
[12]W. Braun, R. Shayduk, T. Flissikowski, M. Ramsteiner, H. T. Grahn, H. Riechert, P. Fons, and A. Kolobov, Appl. Phys. Lett. **94**, 041902 (2009).
[13]F. Katmis, R. Calarco, K. Perumal, P. Rodenbach, A. Giussani, M. Hanke, A. Proessdorf, A. Trampert, F. Grosse, R. Shayduk, R. Campion, W. Braun, and H. Riechert, Cryst. Growth Des. **11**, 4606 (2011).
[14]A. Shalini, Y. Liu, U. Al-Jarah, G. P. Srivastava, C. D. Wright, F. Katmis, W. Braun, and R. J. Hicken, Sci. Rep. **3**, 2965 (2013).
[15]G. A. Garrett, T. F. Albrecht, J. F. Whitaker, and R. Merlin, Phys. Rev. Lett. **77**, 3661 (1996); M. Hase, K. Mizoguchi, H. Harima, S. Nakashima, M. Tani, K. Sakai, and M. Hangyo, Appl. Phys. Lett. **69**, 2474 (1996); K. Ishioka, M. Kitajima, and O. V. Misochko, J. Appl. Phys. **103**, 123505 (2008).
[16]K. S. Andrikopoulos, S. N. Yannopoulos, A. V. Kolobov, P. Fons, and J. Tominaga, J. Phys. Chem. Solids **68**, 1074 (2007).
[17]DataRay WinCamD-UCD12.
[18]V. V. Kruglyak, R. J. Hicken, M. Ali, B. J. Hickey, A. T. G. Pym, and B. K. Tanner, Phys. Rev. B **71**, 233104 (2005).
[19]M. K. Farr, J. G. Traylor, and S. K. Sinha, Phys. Rev. B **11**, 1587 (1975).
[20]G. C. Sosso, S. Caravati, R. Mazzarello, and M. Bernasconi, Phys. Rev. B **83**, 134201 (2011).
[21]P. Nemec, V. Nazabal, A. Moreac, J. Gutwirth, L. Benes, and M. Frumar, Mater. Chem. Phys. **136**, 935 (2012).
[22]J. Akola, J. Larrucea, and R. O. Jones, Phys. Rev. B **83**, 094113 (2011).
[23]E. Carria, A. M. Mio, S. Gibilisco, M. Miritello, F. d'Acapito, M. G. Grimaldi, and E. Rimini, Electrochem. Solid-State Lett. **14**, H480 (2011).
[24]E. Carria, A. M. Mio, S. Gibilisco, M. Miritello, C. Bongiorno, M. G. Grimaldi, and E. Rimini, J. Electrochem. Soc. **159**, H130 (2012).
[25]P. J. Carroll and J. S. Lannin, Phys. Rev. B **27**, 1028 (1983).
[26]Y. Liu, M. M. Aziz, A. Shalini, C. D. Wright, and R. J. Hicken, J. Appl. Phys. **112**, 123526 (2012).
[27]G. C. Sosso, S. Caravati, C. Gatti, S. Assoni, and M. Bernasconi, J. Phys.: Condens. Matter **21**, 245401 (2009).
[28]B. Liu, Z.-T. Song, T. Zhang, S.-L. Feng, and B. Chen, Chin. Phys. **13**, 1947 (2004).